Water Air Soil Pollut (2009) 199:323–341
DOI 10.1007/s11270-008-9882-x

Environmental Impact of Mining Activities in the Southern Sector of the Guadiana Basin (SW of the Iberian Peninsula)

J. Delgado · A. M. Sarmiento · M. T. Condesso de Melo · J. M. Nieto

Received: 22 February 2008 / Accepted: 27 September 2008 / Published online: 19 October 2008

Abstract The southern sector of the Guadiana River basin (GRB) drains the central-western part of the Iberian Pyrite Belt, an area with many polymetallic sulfide deposits and residues of mining activities that under oxidizing conditions generate an acidic leachate with large quantities of sulfates, metals, and metalloids in solution. These acidic leachates seep into the fluvial system contaminating the surface water bodies and increasing the contamination risk for local populations and riparian habitats. The present study was carried out both in Portugal and Spain with the main aim of identifying the principal contamination sources that produce acid mine drainage (AMD) in the southern part of the GRB and to evaluate the seasonal variations of water quality affected by AMD. The physicochemical parameters determined in the field (temperature, electrical conductivity, pH, redox potential, and dissolved oxygen) are discussed and interpreted together with the hydrochemical analysis of surface water samples collected at 79 points of observation. The data show a strong seasonal variation of surface water quality with poorer water quality standards during the dry season. It is also possible to observe that there is a natural decrease in pollution levels with increasing distance from the pollution source (mining areas). Acidic leachates are gradually neutralized as they drain away from the mining areas depositing Fe-(Cu-Al) bearing secondary minerals. There is also an important contaminant load reduction in the estuary area as a result of the mixing process with seawater. This contributes to a loss of the metals in solution due to both dilution and precipitation, as a result of pH increase.

Keywords Guadiana River basin · Acid mine drainage · Iberian Pyrite Belt · Metal pollution

J. Delgado (✉) · A. M. Sarmiento · J. M. Nieto
Department of Geology, Faculty of Experimental Sciences, University of Huelva,
Campus El Carmen, Avda. Fuerzas Armadas, s/n,
21071 Huelva, Spain
e-mail: joaquin.delgado@dgeo.uhu.es

M. T. Condesso de Melo
Department of Geosciences, University of Aveiro,
3810-193 Aveiro, Portugal

1 Introduction

The southern part of the Guadiana River flows through different materials of the Iberian Pyrite Belt (IPB), one of the most important metal bearing areas in the world (Fig. 1), with around 1,700 million tonnes of original reserve of polymetallic sulfide deposits (Sáez et al. 1999). Polluting acidic leachates, with very high metal and sulfate concentrations, known as acidic mine drainage (AMD), originate from the exploitation of these sulfide deposits. Mining activity in the IPB started in the third millennium B.

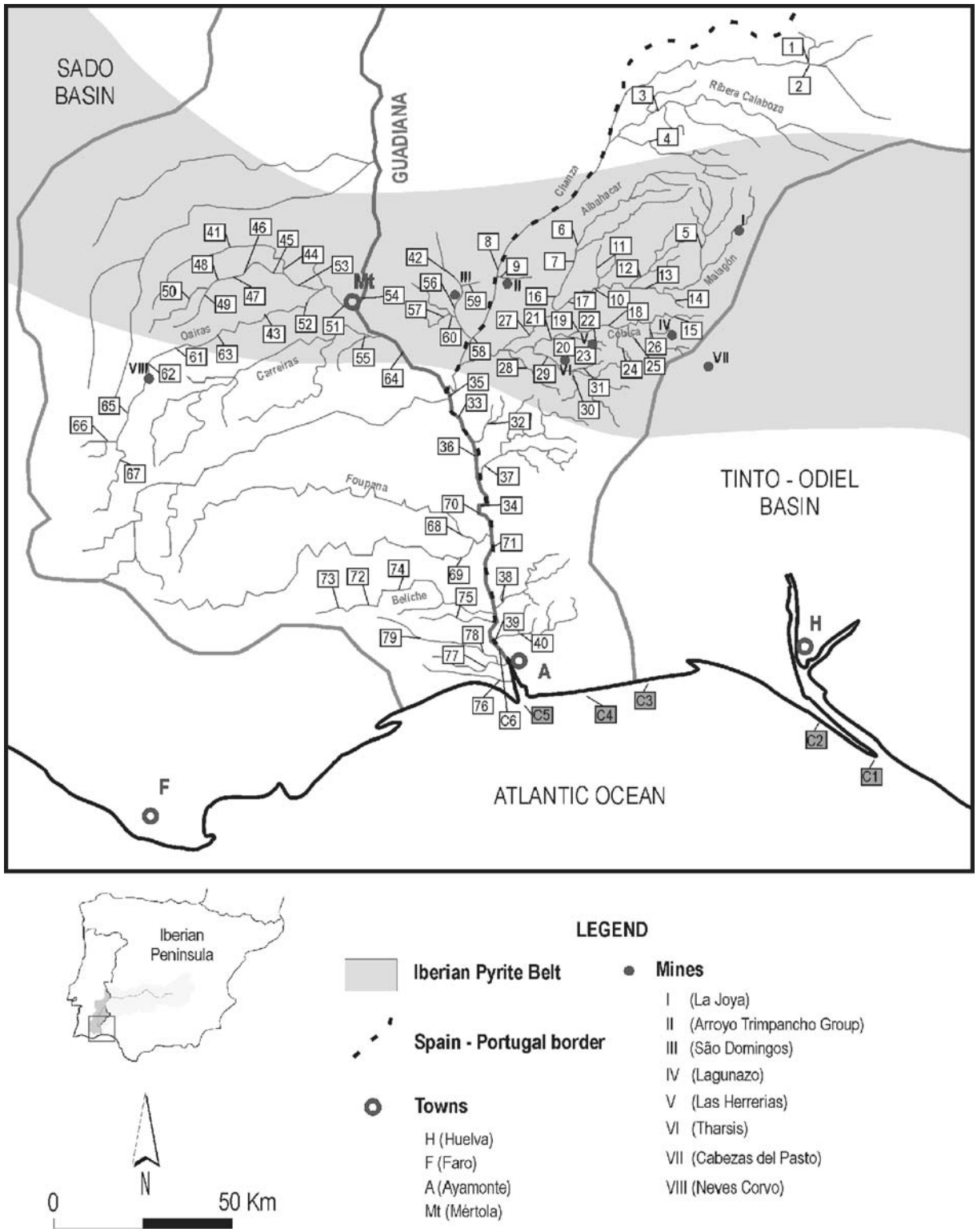

Fig. 1 Map of the lower section of Guadiana basin, showing the sampling points and the main mines of the Iberian Pyrite Belt in this sector

C. (Nocete et al. 2005), and even though today there is a very small number of active mines, the pollution impact of AMD still exists due to both leaching from the large amount of outcropping polymetallic sulfide deposits or from products related to the exploitation of these deposits such as waste piles, residues from the smelting process, ashes, low grade stockpiles, and even from the abandoned underground stopes and chambers.

Some chemical and biochemical reactions take place when pyrite and other sulfides such as galena, sphalerite, arsenopyrite, and chalcopyrite are exposed on surface. There they are subjected to oxidation due to oxygen and water reaction, resulting in a highly polluting lixiviate with high acidity and sulfate concentrations, metals, and metalloids such as Fe, Cu, Zn, Pb, Cd, Mn, and As. The leachate seeps into the fluvial system contributing to the pollution of the surrounding environment and to the degradation of water quality in the southern part of the Guadiana River basin, including the vulnerable estuary area.

There have been numerous research works related to the mining pollution in the study area which have resulted in different publications (Borrego et al. 2002; Grande et al. 2005; Elbaz-Poulichet et al. 2001; Sainz et al. 2002) among others, although the main areas for investigation have been the estuaries of the Tinto and Odiel rivers. Quite recently, a number of investigations have been completed on the Odiel river basin (Olías et al. 2004, 2006; Sarmiento et al. 2004, 2006, 2008) among others, in which the contamination load from the river into the estuary and its impact on the water quality during the dry and wet seasons was estimated. Therefore, the environmental problem derived from acid mine drainage into the Odiel and Tinto rivers in the Huelva area is well known. Acid mine drainage generation and mine-related pollution in the São Domingos area, in the Alentejo (SW Iberian Peninsula, Portugal) is also well known (Freitas et al. 2004; Gerhardta et al. 2004; Bryan et al. 2006; Abreu et al. 2008). However, there are few studies on the pollution due to AMD in the Guadiana basin, integrating both the polluting agents coming from the Spanish and Portuguese basins (Delgado et al. 2006, 2007). That is the reason why it is necessary to compile this investigative work to identify the sources of pollution due to AMD in the southern part of the Guadiana basin and estimate the seasonal variations in the water quality.

2 Description of the Lower Guadiana River Basin

The Guadiana River flows, in this area, through a very gentle valley (Boski et al. 2002), between "Sierra de Aracena" and "El Granado" on the left bank (Huelva province) and "Serra do Caldeirão" on the right bank (Alentejo province) until it reaches the Atlantic Ocean, where an estuary of high ecological importance has developed (Natural Reserve—"Sapal do Castro Marim and Vila Real de Sto. António" and "Marismas del Carreras"). The climate of the lower Guadiana basin is of Mediterranean type, with hot summers and mild winters, when most of the rain falls. December and January are the wettest months (average rainfall discharge up to 78.40–89.26 mm/month) and July and August are the driest months (0.96–2.15 mm/month; Morales 1993). The average rainfall ranges from 500 mm in the lower part of the valley to 1,000 mm in the mountains. The distribution of rainfall, the high average annual temperature (15–20°C), the hours of sun per year (2,800–3,000), and the high potential evapotranspiration values (around 750–950 mm/year) produce a strong seasonal effect (Loureiro 1983; Rivas-Martínez et al. 1990; Morales 1993; Capelo 1996).

The main tributaries to the Guadiana River are on the right bank: the rivers Caia (813 km^2), Degebe (1,527 km^2), Cobres (1,151 km^2), Vascão (462 km^2), Foupana (410 km^2), Oeiras (499 km^2), and Odeleite (773 km^2) and on the left bank: the rivers Ardila (3,634 km^2) and Chanza (1,480 km^2). The Chanza river, which is the main tributary of the Guadiana on its lower part, receives as main tributaries the Barranco de San Marcos stream on the right bank and the Malagón (its main tributaries are the Albahacar and Cobica streams) and Rivera del Calaboza streams on the left bank.

3 Methodology

During the hydrological year 2005/2006, 79 observation points were selected for water sample collection in both the Spanish and Portuguese sectors of the lower Guadiana River basin and other six points in the nearby coastline (Fig. 1). A total of 140 water samples were collected, 30 samples coming from estuarine and marine waters, 26 samples from AMD-contaminated stream waters, and 84 samples from

uncontaminated stream freshwaters. In order to evaluate the seasonal variations in the water quality, two different sampling campaigns were carried out, one after a prolonged dry season (November 2005) and the other after the following wet season (April 2006).

The most important physicochemical parameters were measured in situ. Temperature, electrical conductivity, and pH were measured with portable measuring equipment MX300 (Mettler Toledo). Redox potential (Eh) and dissolved oxygen were measured with HANNA measuring equipment. Eh was measured with a Pt and Ag/AgCl electrode from Crison. Redox potential and pH were properly calibrated on site against supplied calibration standards: Hanna standard solutions (pH 4.01 and 7.01) for pH and Hanna standard solutions (240 and 470 mV) for Eh. The results for redox potential in situ were corrected to give the Eh values that would be obtained with a reference hydrogen electrode (Nordstrom and Wilde 1998).

Water samples were filtered immediately through 0.45 μm filter holders, acidified in the field to pH<2 with HNO_3 (2%) suprapur (Merck), and stored at 4°C in polyethylene containers until analysis. Samples collected for anion and alkalinity determinations were also filtered but not acidified.

Dissolved major cations, S, P, and trace elements were determined by inductively coupled plasma atomic emission spectrometry (ICP-AES; Jobin Yvon ULTIMA 2), in a spectrometer equipped with a cyclonic concentric nebulizer. The method used was designed in order to measure major, minor, and trace elements in waters affected by acid mine drainage (Tyler et al. 2004). Single certified ICP standard solutions from SCP SCIENCE were used for the preparation of calibration multielemental standards. Certified reference material SRM-1640 NIST (freshwater type) and interlaboratory standard IRMM-N3 (wastewater test material, European Commission Institute for Reference Materials and Measurements) were also measured during the study period. Multielemental Reference Standards and blanks were checked at the beginning and at the end of each sequence. Detection limits were calculated by average and standard deviations from ten blanks. Detection limits for major cations were less than 200 μg/L; for trace elements were 50 μg/L for Zn; 5 μg/L for Cu; <3 μg/L for Li, Mo, Se, and Sr; 2 μg/L for As; and 1 μg/L for Al, Cd, Co, Cr, Ni, and Pb.

Anions determinations were carried out by ionic chromatography using a Dionex DX-120 machine fitted with an AS 9-HC of 4×250 mm column and 4 mm ASRS-ULTRA suppressing membrane. Detection limits were 0.1 mg/L for chloride and 0.5 mg/L for sulfate. The alkalinity was determined by the titration method (Standard Methods 2320 for the Examination of Water and Wastewater) with phenolphthalein and bromocresol green indicators.

Multivariate analysis techniques, such as principal components analysis (PCA), aid in reducing the complexity of large-scale data sets and are currently widely used in environmental impact studies (Perona et al. 1999). Thus, the statistical analysis by PCA is a simple but powerful tool to better understand a complex water system and can be used to extract the factors associated with the hydrochemical variability and obtain the spatial / temporal changes in the water quality (Bengraïne and Marhaba 2003). In this way, PCA was carried out by means of a Spearman correlation matrix to the variables and samples (Davis 1986), in order to establish possible polluting agents and relations among polluting agents, as well as the effect of different seasons on the quality of water.

The PHREEQC program (version 2.0; Parkhurst and Appelo 1999) was used for calculating the activity and chemical speciation of dissolved species and the saturation index of minerals [SI = log(IAP/KS), where SI is the saturation index, IAP is the ion activity product, and KS is the solid solubility product] in the parent solutions. The thermodynamic database of PHREEQC was enlarged with data from geochemical code WATEQ4F (Ball and Nordstrom 1991). Solubility constants [KS] from literature were used for other minerals such as schwertmannite. Zero, negative, and positive SI values indicate that the solutions are saturated, undersaturated, and supersaturated, respectively, with respect to a solid phase. For a state of supersaturation, precipitation of the solid phase is expected.

Hence, this theoretical modeling can be compared with the numerous works existing about the chemical speciation of these acid waters and the mineralogical characterization of the sediments in the fluvial courses affected by AMD in the IPB (see for examples Sánchez-España et al. 2005a, 2006b).

4 Results and Discussion

4.1 Statistical Analysis and Hydrochemical Characteristics

The results obtained from the analysis of the waters are characterized by large variations of the physicochemical parameters and composition, which illustrates the great diversity of geochemical conditions in the drainage systems. Table 1 shows the statistical values of the measured parameters in the three types of collected samples: estuarine waters, AMD-uncontaminated freshwaters, and AMD-contaminated freshwaters.

Samples belong to seaside areas or waters from areas which can be affected by the sea tides (estuary of the Guadiana River) show ranges between 7.5 and 8.6 of pH, 0.3 and 51 mS/cm of electrical conductivity, and 150 and 833 mV of redox potential. Maximum concentrations of many "trace" metals are high—for example, As (up to 120 μg/L), Cr (up to 410 μg/L), Fe (up to 2 mg/L), and Ni (up to 428 μg/L; Table 1).

Relating to AMD-uncontaminated freshwaters, these streams are characterized as near-neutral pHs (mean 7.7), and electrical conductivity does not exceed 920 μS/cm. Major anions show values between 15 and 273 mg/L of SO_4^{2-}, up to 320 mg/L of HCO_3^-, and 7.5 and 148 mg/L of Cl^- and average concentration of Al, Fe, Cu, Mn, and Zn below detection limit (Table 1). Characteristics of these waters provide the hydrochemical reference

Table 1 Results of the statistical analysis of the total samples analyzed

	Estuarine and seawaters					AMD-uncontaminated stream freshwaters					AMD-contaminated stream freshwaters				
	n	Me	Max	Min	SD	*n*	Me	Max	Min	SD	*n*	Me	Max	Min	SD
pH	30	8.00	8.58	7.49	0.30	84	7.74	9.30	6.75	0.50	26	4.00	8.71	0.61	2.64
EC (μS/cm)	30	20,134	50,600	270	22,528	84	423	920	101	179	26	4,644	49,500	460	11,019
Eh (mV)	30	446	833	152	203	84	571	870	315	127	22	817	1,124	327	209
Al (mg/L)	30	<dl	<dl	<dl		84	<dl	0.57	<dl	0.08	26	109	727	<dl	199
As (μg/L)	30	24.3	120	<dl	37.9	84	<dl	4.12	<dl	0.79	26	3,041	36,000	<dl	9,715
Ca (mg/L)	30	1,763	9,189	8.30	3,411	84	23.2	71.2	2.70	14.3	26	66.3	192	17.0	56.5
Cd (μg/L)	30	<dl	5.00	<dl	2.00	84	<dl	<dl	<dl		26	92.7	1,247	<dl	249
Co (μg/L)	30	<dl	<dl	<dl		84	<dl	4.47	<dl	0.66	26	490	3,770	<dl	983
Cr (μg/L)	30	50.2	410	<dl	119	84	<dl	31.5	<dl	4.05	26	65.1	674	<dl	161
Cu (μg/L)	30	<dl	<dl	<dl	65.2	84	<dl	93.9	<dl	11.5	26	8,841	74,317	<dl	16,952
Fe (mg/L)	30	0.46	2.00	<dl	0.57	84	<dl	0.93	<dl	0.15	26	815	11,726	<dl	2,689
K (mg/L)	30	126	410	<dl	165	84	4.20	37.0	0.32	4.97	26	6.64	32.3	<dl	7.41
Li (μg/L)	30	60.5	200	<dl	72.7	84	<dl	13.0	<dl	2.25	26	196	1,226	<dl	314
Mg (mg/L)	30	436	1,503	8.07	608	84	15.1	43.0	3.10	6.19	26	74.9	355	11.7	92.3
Mn (μg/L)	30	<dl	<dl	<dl		84	<dl	<dl	<dl		26	10,114	53,655	<dl	13,956
Mo (μg/L)	30	4.35	12.5	<dl	4.82	84	<dl	4.00	<dl	0.88	26	404	5,352	<dl	1,390
Na (mg/L)	30	4,356	14,500	20.6	5,227	84	35.5	84.0	11.0	16.3	26	46.5	105	9.18	22.5
Ni (μg/L)	30	80.1	428	<dl	126	84	5.46	184	<dl	22.7	26	295	2,199	<dl	555
Pb (μg/L)	30	3.06	10.0	<dl	4.24	84	2.49	19.3	<dl	5.03	26	299	2,872	<dl	774
Se (μg/L)	30	120	540	<dl	187	84	<dl	12.6	<dl	2.73	26	34.3	558	<dl	108
Si (mg/L)	30	34.2	211	<dl	63.0	84	3.29	9.60	0.50	1.61	26	15.7	68.0	<dl	17.9
Sr (μg/L)	30	2,527	9,189	38.5	3,533	84	96.8	270	15.0	57.7	26	168	488	62.0	115
Zn (μg/L)	30	8.33	<dl	<dl	14.6	84	<dl	187	<dl	27.1	26	11,032	78,108	<dl	20,762
Cl^- (mg/L)	30	7,493	21,721	24.1	8,884	84	53.9	148	7.49	27.0	26	32.0	150	<dl	43.5
SO_4^{2-} (mg/L)	30	1,437	4,700	13.1	1,602	84	50.4	273	14.6	40.9	26	3,348	35,929	31.9	8,446
HCO_3^- (mg/L)	30	93.5	171	<dl	56.7	84	82.7	320	<dl	52.9	22	39.4	226	<dl	66.9

Min minimum, *Max* maximum, *Me* mean, *SD* standard deviation, <*dl* below detection limit, *n* number of the samples, *EC* electrical conductivity

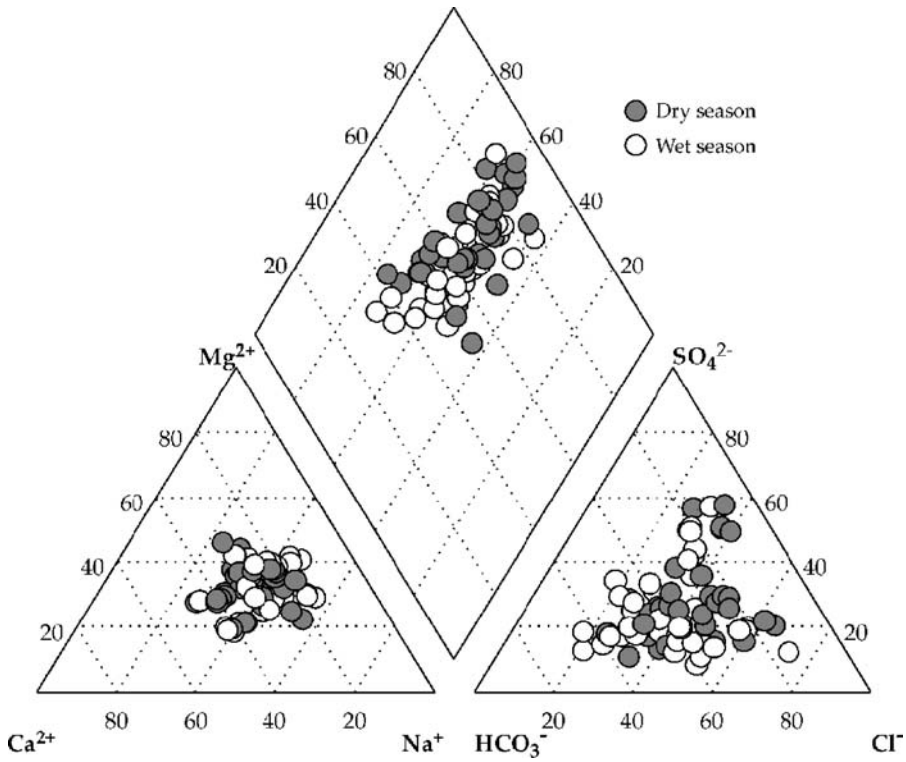

Fig. 2 Piper diagram of uncontaminated freshwater

background for water quality in the area. Two types of water can be differentiated in relation to the hydrochemical facies obtained by the Piper diagram shown in Fig. 2, being sulfate–chloride-mixed type and bicarbonate-mixed waters depending on the localization in the basin.

The last type of samples includes waters from streams affected by AMD (Delgado et al. 2006, 2007). Average values of the measured parameters for this group are showed in Table 1. These waters are characterized by large variations of pH (0.6–8.7), electrical conductivity (0.5–50 mS/cm), and redox potential (327–966 mV). Concentrations up to 727 mg/L of Al, 36 g/L of sulfate, 74 mg/L of Cu, 12 g/L of Fe, 54 mg/L de Mn, 78 mg/L of Zn, 2.9 mg/L of Pb, 2.2 mg/L of Ni, 36 mg/L of As, etc., have been found. The wide range of values in this type of samples indicates the different origins of the streams, with the type of material through which they flow, the time of contact with this material and other physico-

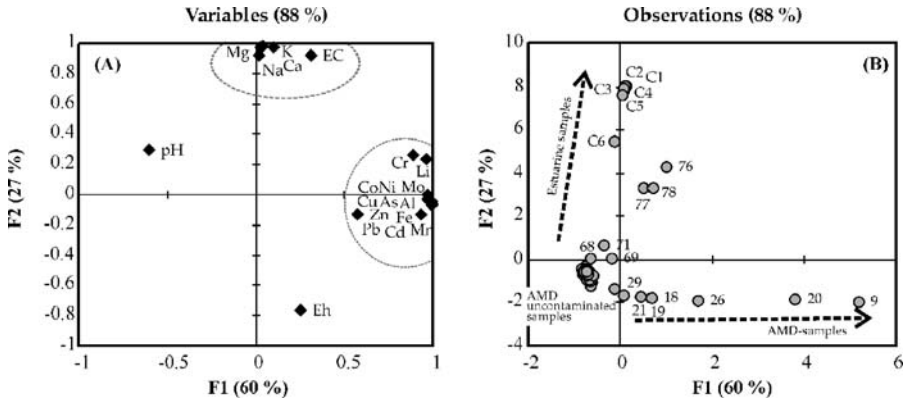

Fig. 3 **a** ACP plot of the variables analyzed and **b** of the sampling points, allowing to distinguish the evolutions according to the physical–chemical characteristics of the water

chemical and biochemical processes, being the factors which determine both their metal composition and acidity.

Principal components analysis was carried out for 23 variables at 85 observation points. Figure 3a shows the results obtained from the PCA analysis of the studied variables. The first factor (F1) accounts for up to 60% of the total variance and is associated with the sulfide oxidation and acid mine generation processes. Similarly, this factor determines the level of the contamination by AMD in the freshwaters according to the pH and the concentration of the toxic metals. The second factor (F2) accounts for 27% of the total variance and is associated with the redox potential and the salinity of the samples due to the marine salts. Figure 3b shows the distribution of the samples regarding to the level of contamination by AMD as well as to the influence of the marine salts.

Figure 4 shows the different types of samples according to the Ficklin diagram (Plumlee et al. 1992) for the composition of mine drainages and natural drainages in mineralized areas. The Ficklin diagram classifies waters based on their pH and the sum of base metals Zn, Cu, Pb, Cd, Co, and Ni. The AMD-contaminated samples are found in the whole range depending on contamination level of the stream. Most of the samples are near neutral and have low metal concentration, including both fresh and estuarine waters. The estuarine samples showing the highest concentration of metals (samples 76, 77, and 78 in Fig. 3b) belong to the area close to the mouth of the Guadiana River (Fig. 1).

Redox potential in the AMD contaminated samples shows a high negative correlation with pH (R^2=0.80;

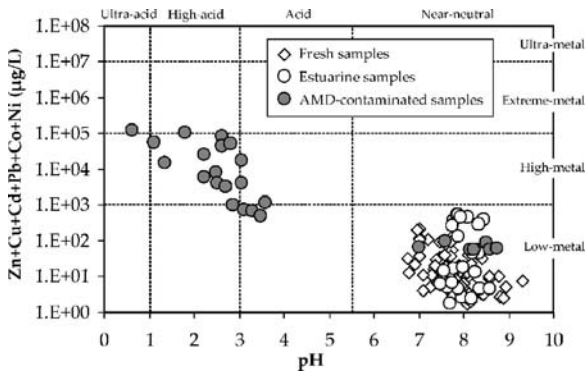

Fig. 4 Ficklin diagram showing the sum of dissolved base metals (Zn, Cu, Cd, Pb, Co, and Ni) for the analyzed samples

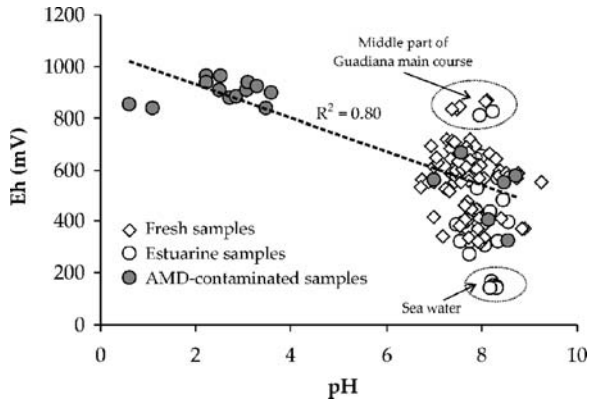

Fig. 5 Relationship between redox potential and pH

Fig. 5), increasing as pH decreases, just as it can see observed in Fig. 3a. Most of the uncontaminated samples (fresh and estuarine waters) have a potential between 200 and 800 mV, with the exception of the samples belonging to the seawaters (redox potential does not exceed 170 mV) and the samples located in the middle part of the main course of the Guadiana River (Eh higher than 800 mV, points 35, 33, 36, 34, 70; Fig. 1). These samples show a redox potential higher, in relation to pH, possibly due to their location close to the mixing zone of the contaminated streams with the main channel of the Guadiana River.

4.2 Seasonal Variations

The Fig. 2 shows the Piper diagram for the uncontaminated fresh samples in two different seasons: dry (November 2005) and wet season (April 2006). In most water streams, a progressive increase in the concentrations due to strong evaporation (generally values over 900 mm) is produced during the dry season. The pH values, as well as bicarbonate, are slightly higher in April, while sulfate and chloride concentration decreases. In November, the composition is less bicarbonate and more chloride–sulfate and the highest concentration of metals such as Fe (930 µg/L), Al (570 µg/L), Zn (190 µg/L), Cu (94 µg/L), and Pb (19 µg/L) can be observed.

Table 2 displays the statistical values of the contaminated samples collected both during the dry and wet seasons. Water samples collected in November after a prolonged drought period show in general slightly lower pH values (average of 3.6) than the samples collected after the wet season (average of

Table 2 Statistical values of AMD-contaminated samples in dry and wet seasons

	Dry season					Wet season				
	n	Me	Max	Min	SD	*n*	Me	Max	Min	SD
pH	13	3.63	8.71	0.61	2.62	13	4.37	8.56	1.08	2.72
EC (μS/cm)	13	5,640	49,500	467	13,259	13	3,647	32,300	460	8,659
Eh (mV)	11	830	964	560	165	11	722	921	327	221
Al (mg/L)	13	129	727	<dl	209	13	89.2	707	<dl	196
As (μg/L)	13	3,172	35,964	<dl	9,883	13	2,911	36,000	<dl	9,946
Ca (mg/L)	13	83.8	192	21.6	61.9	13	48.9	179	17.0	46.5
Cd (μg/L)	13	162	1,247	<dl	343	13	23.9	105	<dl	32.8
Co (μg/L)	13	575	3,770	<dl	1,045	13	405	3,466	<dl	952
Cr (μg/L)	13	80.9	674	<dl	183	13	49.3	522	<dl	143
Cu (μg/L)	13	11,303	74,317	<dl	20,536	13	6,379	46,287	<dl	12,801
Fe (mg/L)	13	978	11,726	<dl	3,231	13	652	7,756	<dl	2,136
K (mg/L)	13	8.00	32.3	<dl	9.30	13	5.28	13.6	0.82	4.90
Li (μg/L)	13	254	1,226	<dl	347	13	137	1,016	<dl	280
Mg (mg/L)	13	97.0	355	17.9	109	13	52.8	262	11.7	69.4
Mn (μg/L)	13	13,654	53,655	<dl	16,016	13	6,573	39,131	<dl	11,051
Mo (μg/L)	13	425	5,352	<dl	1,481	13	383	4,887	<dl	1,353
Na (mg/L)	13	50.9	105	9.18	28.3	13	42.1	66.0	23.0	14.7
Ni (μg/L)	13	360	2,199	<dl	596	13	231	1,927	<dl	527
Pb (μg/L)	13	259	2,861	<dl	784	13	339	2,872	<dl	794
Se (μg/L)	13	17.0	95.4	<dl	25.5	13	51.6	558	<dl	152
Si (mg/L)	13	18.4	52.2	0.30	18.0	13	13.0	68.0	<dl	18.2
Sr (μg/L)	13	201	444	77.8	112	13	134	488	62.0	112
Zn (μg/L)	13	19,115	78,108	<dl	26,420	13	2,950	26,000	<dl	7,649
Cl^- (mg/L)	13	35.6	150	<dl	53.3	13	28.3	88.8	<dl	32.7
SO_4^{2-} (mg/L)	13	4,133	35,929	63.0	9,693	13	2,563	26,784	31.9	7,303
HCO_3^- (mg/L)	11	39.9	226	<dl	74.9	11	38.9	176	<dl	61.5

Min minimum, *Max* maximum, *Me* mean, *SD* standard deviation, <*dl* below detection limit, *n* number of the samples, *EC* electrical conductivity

4.4), which means that there is a lower neutralizing capacity of the AMD during the summer months. Electrical conductivity and redox potential are also higher in dry season, pointing out bigger oxidant conditions and higher concentrations in most of the ions.

The strong evaporation during the dry season causes the precipitation of soluble efflorescents sulfates in the river courses affected by AMD. These soluble minerals (i.e., melanterite and copiapite) store acidity and toxic metals (Fe, Al, Cd, Co, Cu, and Zn) during the dry season (Olías et al. 2004). In the wet season, drainage waters dissolve the acid salts precipitated during the summer, and for this reason immediately after the first rainfalls and in the vicinity of the AMD area, concentrations of metals in the waters may be very high (Cánovas et al. 2007). However, as water flows and transport and dilution of the contaminant occurs, the contaminant load in the water samples collected during this season in the lower Guadiana River basin decreases.

Concentrations of elements in AMD-affected waters such as As, Pb, Cr, Cd, and Cu are regulated by precipitation of Fe-rich materials, which may adsorb or coprecipitate these toxic elements during the flow of these streams (Hudson-Edwards et al. 1999). Such associations with Fe-rich materials have particularly been indicated as a regulation mechanism of toxic element contents in the environment. Figure 6 shows the relationship between pH and Cu/Fe (Fig. 6a) and Mn/Fe (Fig. 6b) ratios. The ratios are lower in the wet season because the pH is higher and both the precipitation of Fe-minerals and the absorption processes are favored. On the contrary, the mobility in water is higher in the dry season and the ratio metal/Fe increases.

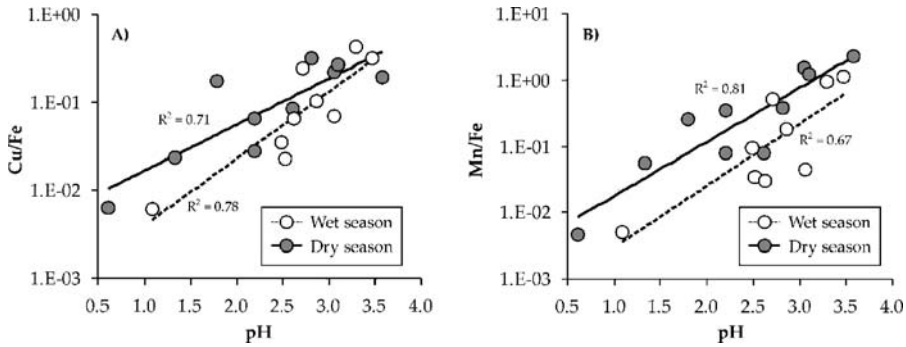

Fig. 6 Plot of **a** Cu/Fe ratio and **b** Mn/Fe ratio against pH for the contaminated samples

4.3 AMD Leaches

4.3.1 General Location of Polluting Agents in the Basin

The main areas of pollution due to AMD are located inland, where the mining areas are located, especially near the mines of "Neves Corvo", "São Domingos", "Trimpancho" Group, "Las Herrerías", "Cabezo del Pasto", "El Lagunazo", and "Tharsis" (Fig. 1). These areas are the main pollution sources for the streams related to the leaching of polymetallic sulfides. These samples have been described in Section 4.1 as belonging to affect by AMD. However, it is proven, for every case, that there is a reduction in the polluting content as we move away from the contamination source. This is due to the dilution effect after the mixing with freshwaters (Fig. 7) and estuarine waters, which contributes to a gradual increase in the pH of the mixture and, as a consequence, to the loss of mobility of the metals in solution in the main channel of the Guadiana river (Fig. 8). Among the streams affected by AMD, two have been identified as of greater importance for the water quality in the lower Guadiana—the Cobica stream in Spain that drains two of the main mines of the Spanish sector ("El Lagunazo" and "Las Herrerías") and the S. Domingos stream that drains away the AMD from the S. Domingos mine in Portugal into the Chanza and Guadiana rivers.

A more detailed study of these areas has been carried out to characterize the evolution of the content in potentially contaminant elements. The detailed location of the sampling points is illustrated in Fig. 9, the initial conditions of the samples have been illustrated in the Table 3, and the results obtained of the hydrochemical model developed with PHREEQC have been detailed in the figures following this section.

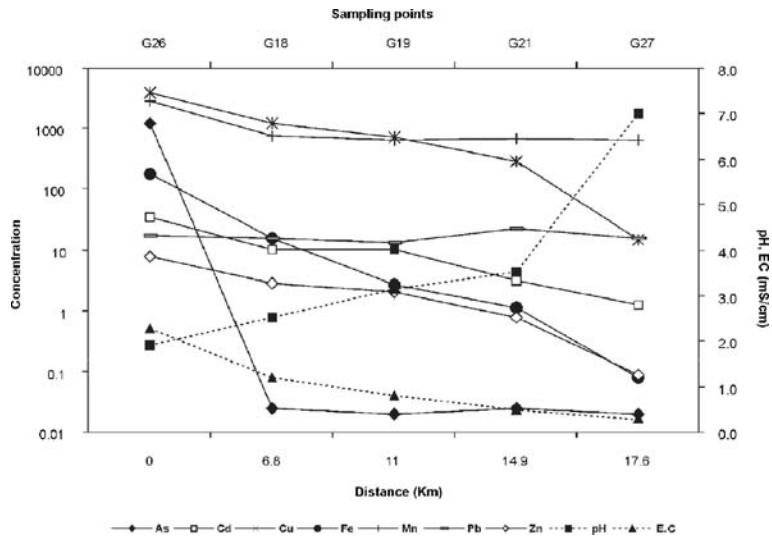

Fig. 7 Examples of the spatial evolution of the physical–chemical parameters of the water samples in stream affected by acid drainage mine from the lower section of Guadiana basin. *EC* electrical conductivity (mS/cm), concentration (mg/L from Cu, Fe, Mn, and Zn, and μg/L for the rest)

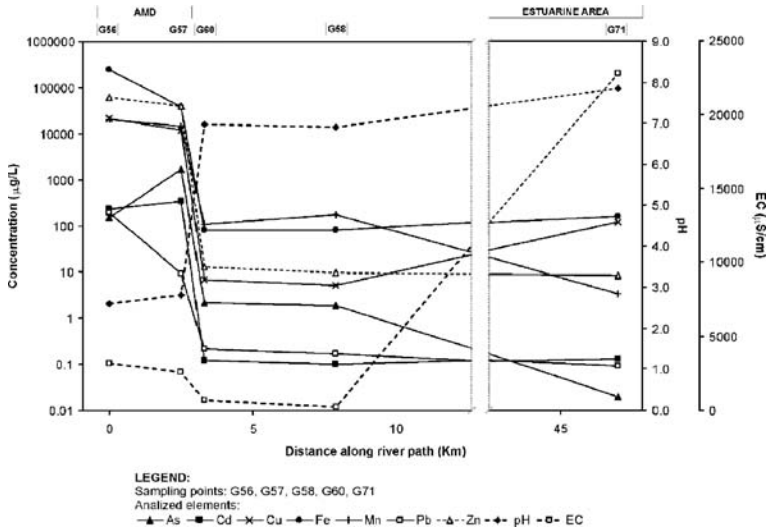

Fig. 8 Spatial evolution of the physical–chemical parameters of the water samples in the S. Domingos stream, showing the evolution of the parameters up to the estuarine area

4.3.2 Main Species Dissolved in the Contaminated Waters of the Cobica and S. Domingos Streams

To characterize the species whose thermodynamic precipitation is possible, a study has been carried out using the code PHREEQC (Parkhurst and Appelo 1999) of the Cobica and S. Domingos streams (main areas affected by AMD). In this study, the ionic activities and saturation indexes of the mineral assemblages typical of these mining environments have been determined with chemical data composition.

In this sense, the main solid phases result of precipitation from dissolved species in acid environments have been widely discussed (Carlson and Schwertmann 1981; Bigham et al. 1990, 1994, 1996; Nordstrom and Alpers 1999; Yu et al. 1999; Kawano and Tomita 2001; Williams et al. 2002; Dold 2003; Jerz and Rimstidt 2003; Murad et al. 2003; Regenspurg et al. 2004). In the IPB, the most abundant Fe-bearing phases are ferrihydrite and schwertmannite, in addition to jarosite and goethite (Sánchez-España et al. 2005a). These Fe(III) phases traditionally has been referred to under ambiguous terms such as "ochreous precipitates", "amorphous iron oxides", "ferric hydroxides", or "poorly crystalline oxyhydroxides". The "ochreous precipitates" also include oxyhydroxides and oxyhydroxysulfates of Al, such as jurbanite, alunite, basaluminite, gibbsite, and amorphous oxyhydroxides (Blowes and Ptacek 1994; Nordstrom 1982; Nordstrom and Alpers 1999; Bigham and Nordstrom 2000; Sánchez España et al. 2005a, b, 2006a, b) that can play an important role in the control of the geochemical evolution of acidic waters.

Figure 10 illustrates mean values of the main Fe, Al, and Cu species in the Cobica stream in two seasons, dry and wet. Fe species show interesting differences between the two seasons (dry and wet). During the dry season, Fe (III) species (Fe^{3+}, $FeSO_4^{+}$, $FeOH^{2+}$, $FeHSO_4^{2+}$, and $FeOH_2^{4+}$) are predominant (Fig. 10), while Fe (II) species (Fe^{2+}) only represent 15% of the whole. Likewise, in the wet season, $FeSO_4^{+}$ represents 52% of the total and the molar concentration of Fe (III) species increases to 80% of the total. The main difference between the two seasons is the increase in sulfurous species in the wet station and a decrease in Fe (III) in the solution.

The most abundant Al species show important differences depending of the season, thus aluminum oxyhydroxides ($AlOH_4^{-}$, $AlOH_2^{+}$) dominate in solution in the dry season (approximately 100%). These are replaced by sulfated species such as $AlSO_4^{+}$, along with Al^{3+} in the wet season (38% and 58%, respectively; Fig. 10).

In the wet season, approximately 100% Cu species correspond to Cu (II), and the predominant species are $CuSO_4$ and Cu^{2+} representing 94% of the whole (Fig. 10). Nevertheless, other minority species exist, such as $CuCl^{+}$, $CuOH^{+}$, and $CuOH_2$. These minority species appear in the dry season in a very low proportion, and therefore, they were not considered relevant, so approximately 100% of the species are formed by Cu^{2+} and $CuSO_4$.

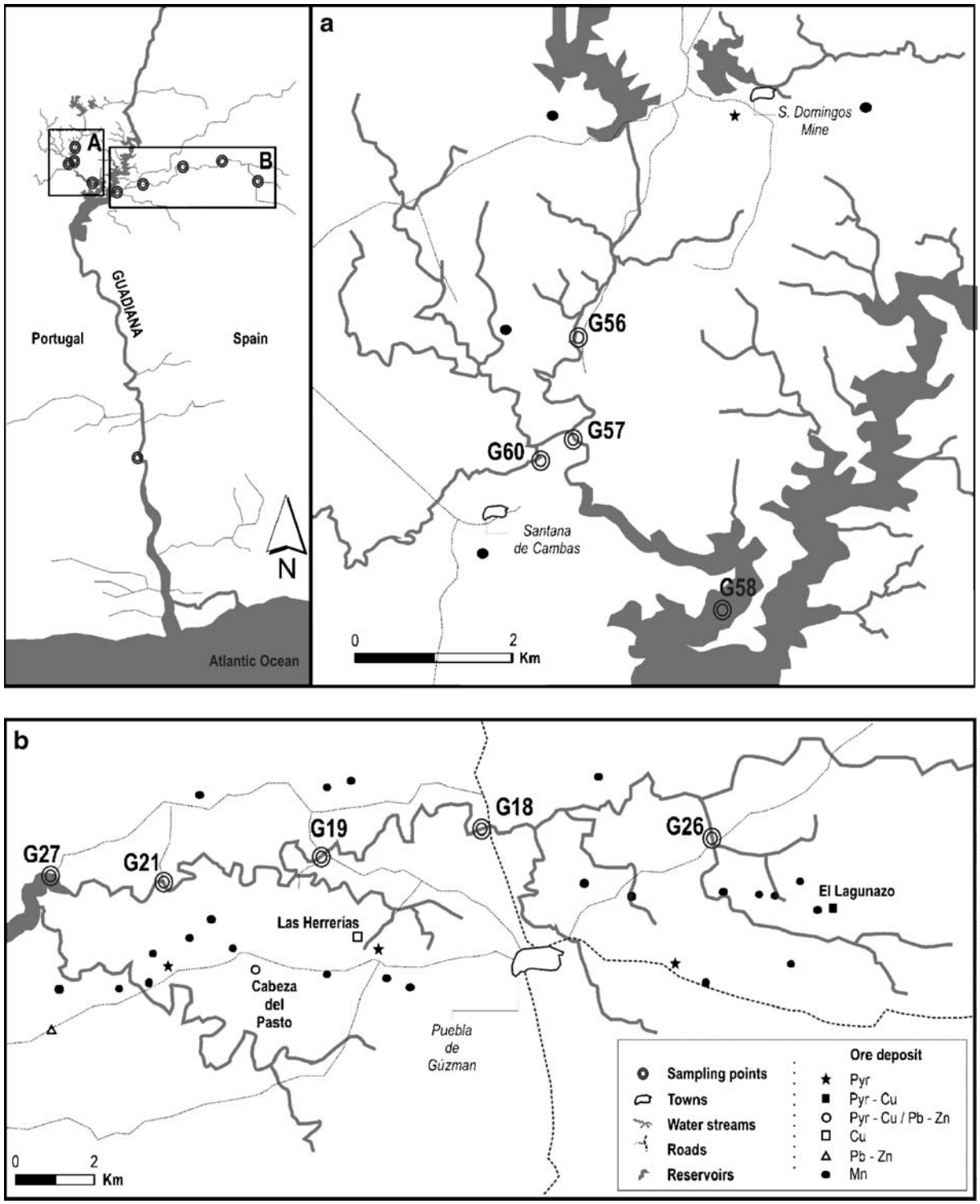

Fig. 9 Detail of the water samples collected in the S. Domingos stream (**a**) and the Cobica River (**b**)

Table 3 Trace elements and main anions concentration of the samples selected for the PHREEQC modeling

Input data	Cobica stream										S. Domingos stream									
	G26d	G26w	G18d	G18w	G19d	G19w	G21d	G21w	G27d	G27w	G56d	G56w	G57d	G57w	G60d	G60w	G58d	G58w	G71d	G71w
Ph	1.3	2.5	2.2	2.9	3.1	3.3	3.6	3.5	7.0	7.0	2.6	2.6	2.8	3.1	7.0	8.1	6.9	7.0	7.9	7.6
pe	19.0	16.3	16.3	14.9	15.4	15.6	15.2	14.1	9.4	9.5	16.0	16.0	16.0	16.0	9.8	6.9	9.7	7.1	9.9	3.5
T^a (°C)	14.0	24.3	15.2	20.2	12.3	22.6	13.2	20.0	14.1	22.0	11.4	23.8	12.0	22.8	15.7	22.3	17.0	21.2	15.8	18.8
Ca	71.5	28.0	54.8	22.0	38.2	22.0	21.6	20.0	19.0	17.0	152	93.7	192	50.0	52.6	24.5	15.6	13.5	142	19.3
Mg	42.4	23.0	34.4	15.0	27.6	15.0	18.5	16.0	14.0	13.0	139	74.4	142	37.0	30.1	13.8	11.5	8.7	400	13.1
Na	9.18	34.0	31.6	33.0	31.8	33.0	25.7	23.0	23.0	21.0	74.5	61.4	56.1	34.6	48.3	36.6	18.7	18.0	3,640	39.8
K	13.9	13.6	4.51	2.31	4.10	1.94	3.77	3.05	3.40	3.40	<d.l	0.8	0.70	1.29	2.57	1.45	2.35	2.19	204	3.69
Fe	189	170	23.6	8.70	4.03	1.40	0.96	1.30	0.11	0.13	249	248	37.5	71.3	0.11	0.09	0.10	0.09	0.16	0.14
Mn	<d.l	5.90	<d.l	1.50	<d.l	1.30	<d.l	1.41	<d.l	<d.l	19.9	7.27	14.30	3.15	<d.l	<d.l	<d.l	<d.l	<d.l	<d.l
Si	11.0	8.70	12.0	5.60	12.9	6.20	2.37	3.00	0.86	1.50	50.0	25.1	31.0	13.0	5.9	3.00	0.90	2.70	0.90	2.50
Cl^-	<d.l	<d.l	<d.l	<d.l	<d.l	<d.l	<d.l	<d.l	32.4	33.4	150	48.3	55.3	49.4	54.7	56.8	28.9	29.3	4,420	68.4
HCO_3^-	–	–	–	–	–	–	–	–	34.7	22.3	–	–	–	–	88.0	106.0	48.0	39.0	140	105
SO_4^{2-}	1,259	831	615	216	423	177	191	150	93	84	3,640	1,813	3,600	741	198	32.5	48.4	48.7	4,700	31.3
Al	57.2	19.0	31.7	5.30	20.4	4.50	2.28	2.53	0.04	0.03	240	223	163	73.9	0.004	0.003	0.001	0.001	0.001	0.002
As	2.44	0.96	0.03	0.02	0.03	0.01	0.03	0.02	<d.l	<d.l	0.15	0.20	1.67	0.16	0.002	<d.l	<d.l	<d.l	<d.l	0.002
Cd	0.05	0.03	0.02	0.01	0.02	0.05	0.003	0.003	<d.l	<d.l	0.23	0.11	0.33	0.06	<d.l	<d.l	<d.l	<d.l	<d.l	<d.l
Cu	0.004	3.82	0.002	0.88	0.001	0.58	<d.l	0.40	0.01	0.02	21.2	15.9	12.0	4.94	0.007	<d.l	0.005	0.03	0.12	0.01
Li	0.18	0.04	0.11	0.02	0.10	0.02	0.02	0.01	0.01	<d.l	0.52	0.34	0.38	0.13	0.002	<d.l	<d.l	0.004	0.06	0.003
Ni	0.16	0.08	0.09	0.02	0.08	0.02	0.03	0.02	0.01	<d.l	0.52	0.26	0.39	0.11	0.01	<d.l	0.006	0.003	0.43	0.001
Pb	0.01	0.02	0.01	0.02	0.01	0.01	0.03	0.02	0.01	<d.l	0.19	0.74	0.01	0.50	<d.l	<d.l	<d.l	<d.l	<d.l	<d.l
Zn	0.01	0.01	<d.l	<d.l	<d.l	<d.l	<d.l	<d.l	0.09	0.09	62.2	26.0	39.3	11.8	<d.l	<d.l	<d.l	0.19	<d.l	<d.l

Units are in ppm. pe is calculated from Eh_H value

<d.l below detection limit

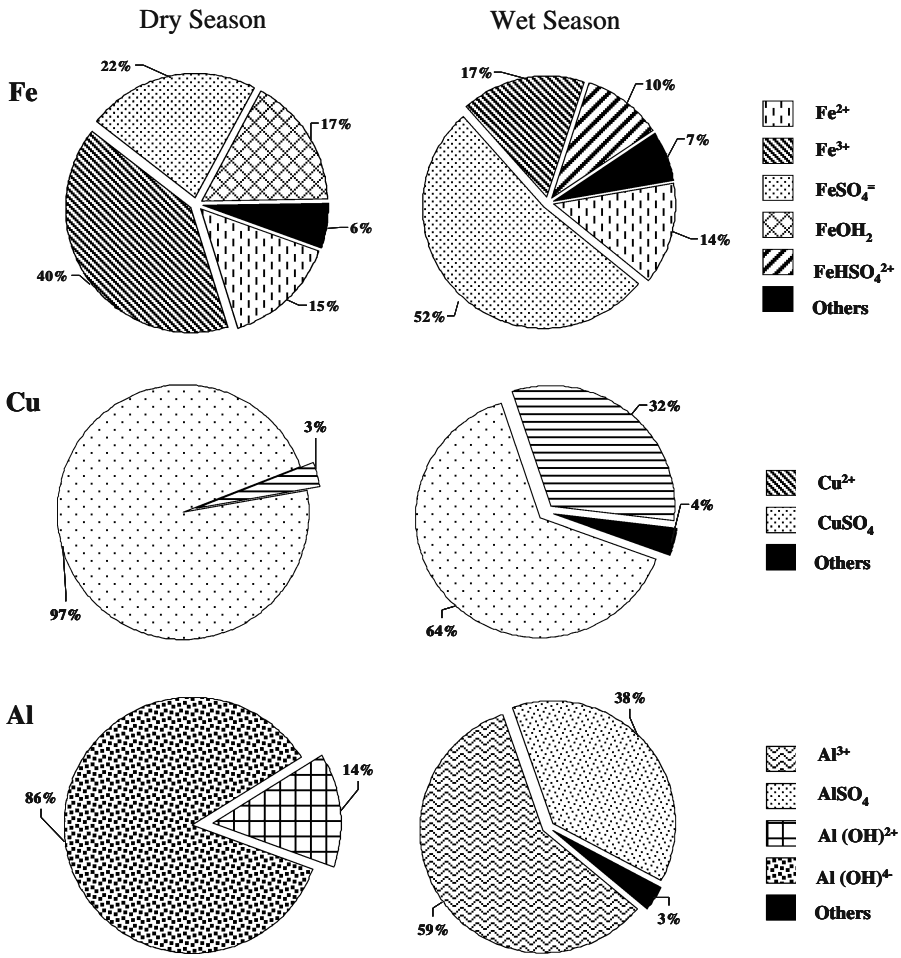

Fig. 10 Mean values of main Fe, Cu, and Al species in the Cobica stream in two different seasons, dry and wet (others represent the minority species slightly relevant in solution)

Geochemical calculations of dissolved species done with PRHEEQC (Fig. 10) illustrate the typical conditions of AMD-affected environments in the IPB. The results show a higher abundance of sulfate complexes ($FeSO_4^+$, $FeHSO_4^{2+}$, $AlSO_4^+$) over trivalent metals (Fe^{3+}, Al^{3+}) in solution, as it has been shown by Sánchez España et al. (2006b) from some streams in the Odiel river basin. However, a detailed analysis reveals that in the wet season (pH increases), the concentration of these sulfate complexes increases over of hydroxide forms ($FeOH^{2+}$, $FeOH_2^{4+}$, $AlOH_4^-$, $AlOH_2^+$). This phenomenon can be due to the dissolution of the soluble efflorescents sulfates precipitated during the summer (Cánovas et al. 2007).

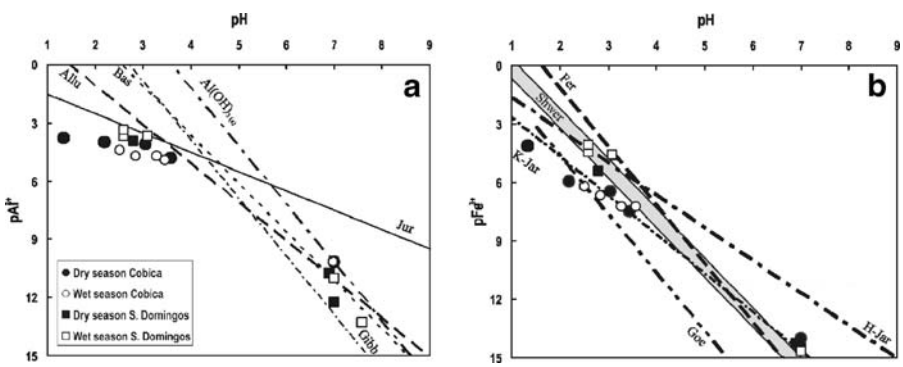

Fig. 11 Representation of the relation among pAl^{3+} and pFe^{3+} vs. pH of the samples analyzed in the Cobica and S. Domingos streams

4.3.3 Saturation Index

The Al minerals which can control Al solubility in acidic waters are jurbanite ($Al(SO_4)OH: 5H_2O$), alunite ($KAl_3(SO_4)_2OH_6$), basaluminite ($Al_4(SO_4)_2OH_{10}: 5H_2O$), and gibbsite microcrystalline (Al_2OH_3) or amorphous ($AlOH_3$; Nordstrom 1982). Jurbanite is the most stable at low pH values (<4) and alunite, basaluminite, and aluminum hydroxides would progressively take on special significance as pH increases (Nordstrom and Alpers 1999). However, despite its apparent thermodynamic stability, jurbanite is not so important as Al solubility control in mining acidic waters, and this mineral barely precipitates in these environments (Bigham and Nordstrom 2000; Blowes and Ptacek 1994).

Figure 11a, where the relation between pAl^{3+} and the pH of the samples analyzed in the Cobica stream has been represented, shows a similar behavior to that described in the previous lines. Thus, at a pH lower than 4, it seems that a harmonious distribution pattern is present with the stability line of the alunite, while with increasing pH, the samples will tend to be progressively aligned with the $AlOH_3$ (amorphous) curve of solubility. Nevertheless, when the pH is extremely low (<3), there is no control in the solubility of Al, since Al tends to be maintained in solution as dissolved species (Al^{3+}). In this sense, Sánchez España et al. (2005a) suggest basaluminite (or its precursor hydrobasaluminite) as the most probably Al mineral phase precipitating at pH around 4.5, in the Odiel River, when acidic lixiviates are neutralized as a result of the dilution by nonacidic waters. This statement agrees with Nordstrom (1982), who suggests that basaluminite is the stable phase in a range of pH of 3.3–5.7.

It is important to mention that there is a deficit of sampling points between pH 4 and 7 due to a sharp increase in the pH downstream that allows us to corroborate that the pattern of the samples is harmonious with that described by Nordstrom and Alpers (1999). However, the distribution of the samples when the pH is over 7 seems to indicate an alignment of these with the stability line of the amorphous oxyhydroxide (AlOH (a) in the graphic).

Given these premises, the minerals that have positive saturation index and that therefore can be stable from a thermodynamic point of view, for the present case study, are alunite, basaluminite, $Al(OH)_3$ amorphous, and diaspore (AlO(OH)). The control of the Al solubility by these minerals can occur between points 21 and 27 for the Cobica stream and points 60 and 71 for the S. Domingos stream as a consequence of the strong dilution by freshwaters and the increase in pH from acid conditions to over neutral conditions (Fig. 12a). The control of the Al solubility may probably be carried out by alunite in ranges of pH 3–4, while at higher pH, the control would be exercised by amorphous aluminum oxyhydroxide.

Fig. 12 Diagrams showing the most relevant mineral saturation indexes obtained for water samples of the Cobica and the S. Domingos streams ▶

Fe oxyhydroxide sulfates, which are formed from mining acidic waters, due to its low crystallinity have been traditionally named as amorphous iron oxides or ferric hydroxides. These minerals are mainly formed by K-jarosite ($KFe_3(SO_4)_2(OH)_6$), ferrihydrite ($Fe_5(OH)_8: 4H_2O$), and schwertmannite ($Fe_8O_8(OH)_6(SO_4$; Cánovas et al. 2007).

In the dry season, the Fe solubility is not controlled by these minerals but by oxides of Cu-Fe as cupric ferrite ($CuFe_2O_4$) and cuprous ferrite ($CuFeO_2$) that seem to play an important role in the control of the concentrations of Fe and Cu, since its precipitation is thermodynamically possible in all streams after sampling points 18 and 57 for the Spanish and Portuguese sectors, respectively (Fig. 12c).

The saturation indexes show the presence of ferrihydrite at point 27, where the pH is around 7 (Murad and Rojik 2003). However, the solubility of this mineral is still being discussed due to its compositional variability, the instability of ferrihydrite and schwertmannite compounds which are quickly transformed into goethite, the presence of sulfates in the crystal latice and as absorbed species, etc. (Yu et al. 1999).

Likewise, goethite has positive saturation index in all cases, but according to the statements of Murad and Rojik (2003), probably only its haste is produced where the pH is found in the range 5–7 (at point 27 of Cobica stream). However, goethite does not appear usually as a direct precipitate from AMD due to its precipitation kinetics, but it is formed by transformation from the before mentioned Fe oxyhydroxide sulfates (Acero et al. 2006; Bigham et al. 1996; Nordstrom and Alpers 1999). Other minerals that seem to control, in the dry season, the solubility

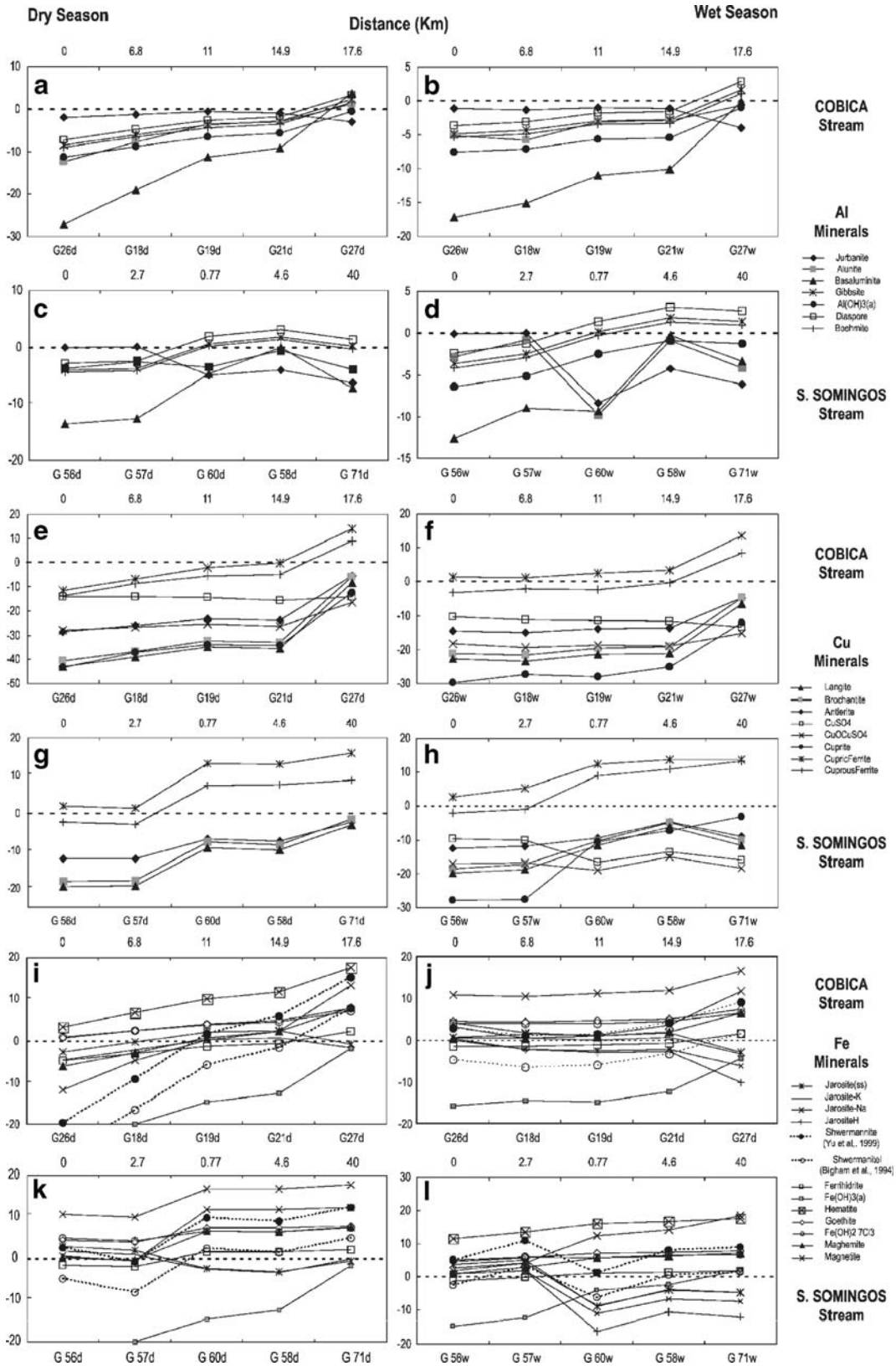
Dry Season
Distance (Km)
Wet Season
0 6.8 11 14.9 17.6
a
b
COBICA Stream
Al Minerals
Jurbanite
Alunite
Basaluminite
Gibbsite
Al(OH)3(a)
Diaspore
Boehmite
G26d G18d G19d G21d G27d
G26w G18w G19w G21w G27w
0 2.7 0.77 4.6 40
c
d
S. SOMINGOS Stream
G 56d G 57d G 60d G 58d G 71d
G 56w G 57w G 60w G 58w G 71w
e
f
COBICA Stream
Cu Minerals
Langite
Brochantite
Antlerite
CuSO4
CuOCuSO4
Cuprite
CupricFerrite
CuprousFerrite
g
h
S. SOMINGOS Stream
i
j
COBICA Stream
Fe Minerals
Jarosite(ss)
Jarosite-K
Jarosite-Na
JarositeH
Shwermannite (Yu et al., 1999)
Shwermannite (Bigham et al., 1994)
Ferrihidrite
Fe(OH)3(a)
Hematite
Goethite
Fe(OH)2.7Cl0.3
Maghemite
Magnesite
k
l
S. SOMINGOS Stream

of Fe are jarosite (ss) and K-jarosite. This occurs when the concentration in the water is higher and only in extremely acid conditions (points G26, G56, and G57 with pH<2.5; Fig. 12i, k). Nevertheless, the saturation index of jarosite depended on the solubility constant used, which differs greatly according to different authors (Baron and Palmer 1996). According to Fig. 11b, where pFe^{3+} vs. pH has been represented, we can verify that, in the dry season, Fe solubility does seem to be controlled by jarosite, but also other minerals may be controlling this solubility.

The saturation index of schwertmannite depended on the thermodynamic constant used; therefore, this has been calculated with the values from constant pK defined by Bigham et al. (1996) and Yu et al. (1999), 18 and 10.5, respectively. Beginning with expression 1, where IAP is the product of activities from ions involved in the reaction of schwertmannite formation (expression 2), opening up IAP in expression 2 and replacing in expression 1 will obtain expression 3.

$$\mathrm{IS} = \log\ \mathrm{IAP} - \log \mathrm{K} \tag{1}$$

$$\mathrm{Fe_8O_8(OH)_{8-2x}}\left(\mathrm{SO_4^{2-}}\right)_x + (24-2x)\mathrm{H}+ = 8\mathrm{Fe^{3+}} + x\mathrm{SO_4^{2-}} + (16-2x)\mathrm{H_2O} \tag{2}$$

$$\mathrm{IS} = 8\log \mathrm{Fe^{3+}} + x\mathrm{pSO4^{2-}} - (24-2x)\mathrm{pH} - \mathrm{Log\ K} \tag{3}$$

To adjust the stoichiometry of the reaction, the value x=1.84 proposed by Acero et al. (2006) has been used. The rest of values in expression 3 have been obtained through the hydrochemical model performed with the PHREEQC code.

The results of this calculation show that, in general, schwertmannite only presents SI greater than zero in extremely acid conditions, with high concentrations of Fe in solution. The curve according to Yu et al. (1999) shows a sharp decrease from values close to 20 at point G26d, passing through a value close to 3 (G18d), to very negative values at the rest of the points. Likewise, this evolution for the values of SI is observed if they are calculated using pK=18 (Bigham et al. 1996), though from point G18d, all the values obtained are negatives (i.e., Fig 12i).

Finally, the control of Cu solubility (Fig. 12e–h) is exercised by oxyhydroxysulfates such as antlerite, brochantite, and langite in both seasons (dry and wet). The possible precipitation from these species (SI>0) occurs always at sampling point 27, because the physical–chemical characteristic of the water changes from acid condition to neutral-alkaline condition (pH=3.05 → pH=7.02).

On the other hand, the water is saturated in kaolinite ($Al_2Si_2O_5(OH)_4$), like in other aluminosilicates at sampling point 27. Oversaturated values can usually be found in high floods, when the pH rises. As usual in other rivers affected by AMD, water also is oversaturated in silica, as shown by chalcedony, cristoboline, and SiO_2 (ss) positive SI.

5 Conclusions

The waters of the lowest part of the Guadiana River show AMD affection. The most important concentrations of almost all potential pollutants have been registered in the Chorrito creek, nearby "Las Herrerías" mine, and, consequently, in the Cobica River where its waters flow, as well as in the S. Domingos creek that drains the S. Domingos mine. Significant Zn concentrations have also been found nearby the mines of "Grupo del Arroyo Trimpancho".

The PCA technique allows distinguish characteristics due to natural influences from anthropogenic ones. Thus, three types of water can be recognized in the lower basin of Guadiana according to its physicochemical characteristics: waters influenced by the sea (estuary of the Guadiana River), nonpolluted freshwaters, and freshwaters affected by AMD pollution (anthropogenic influence).

The analysis of seasonal data shows the improvement of the acid water quality in the wet season. The dilution of the concentrations of As, Co, Ni, and Pb, due to rainfall, the increasing distance from the pollutant source, and the mixing with seawater in the estuarine area favors the low concentration of the polluting elements in the estuary of the Guadiana River.

The analysis of the saturation indexes shows that AMD waters are mainly oversaturated in oxyhydr-

oxide sulfates of Fe and Al; jarosite (ss) and K-jarosite can be present when the metal concentration in the water is high and only in extremely acidic conditions (pH<2.5). Schwertmannite precipitates when the pH is higher than 2.8 and ferrihydrite with slightly higher acid pH values. Finally, basaluminite, gibbsite, and diaspore precipitate when the pH is neutral or near neutral.

Acknowledgements This study has been financed through the project "Monitoring and environmental management of the Guadiana estuary wetlands" (UTPIA), financed by the UE-INTERREG IIIA program and by the Spanish Ministry of Education and Science through the projects CTM2006-28148-E and CTM2007-66724-C02-02.

References

Abreu, M. M., Tavares, M. T., & Batista, M. J. (2008). Potential use of Erica andevalensis and Erica australis in phytoremediation of sulphide mine environments: São Domingos, Portugal. *Geoexploration*, *96*, 210–222.

Acero, P., Ayora, C., Torrento, C., & Nieto, J. M. (2006). The behaviour of trace elements during schwertmannite precipitation and subsequent transformation into goethite and jarosite. *Geochimica et Cosmochimica Acta*, *70*, 4130–4139. doi:10.1016/j.gca.2006.06.1367.

Ball, J. W., & Nordstrom, D. K. (1991). User's manual for WATEQ4F, with revised thermodynamic data base and test cases calculating speciation of major, trace and redox elements in natural waters. *US Geological Survey Open-File Report* 91–183.

Baron, D., & Palmer, C. D. (1996). Solubility of jarosite at 4–35°C. *Geochimica et Cosmochimica Acta*, *60*, 185–195. doi:10.1016/0016-7037(95)00392-4.

Bengraïne, K., & Marhaba, T. F. (2003). Using principal component analysis to monitoring spatial and temporal changes in water quality. *Journal of Hazardous Materials*, *B100*, 179–195. doi:10.1016/S0304-3894(03)00104-3.

Bigham, J. M., Carlson, L., & Murad, E. (1994). Schwertmannite, a new iron oxyhydroxysulfate from Pyhlsalmi, Finland, and other localities. *Mineralogical Magazine*, *58*, 641–648.

Bigham, J. M., & Nordstrom, D. K. (2000). Iron and aluminium hydroxysulfates from acid sulfate waters. In C. N. Alpers, J. L. Jambor (Eds.), *Sulfate minerals. Crystallography, geochemistry, and environmental significance. Reviews in mineralogy and geochemistry, 40* (pp. 351–403). Washington, DC: Mineralogical Society of America.

Bigham, J. M., Schwertmann, S., Carlson, L., & Murad, E. (1990). A poorly crystallized oxyhydroxysulfate of iron formed by bacterial oxidation of Fe(II) in acid mine waters. *Geochimica et Cosmochimica Acta*, *54*, 2743–2758.

Bigham, J. M., Schwertmann, S. J., Traina, S., Winland, R. L., & Wolf, M. (1996). Schwertmannite and the chemical modelling of iron in acid sulfate waters. *Geochimica et Cosmochimica Acta*, *60*, 2111–2121. doi:10.1016/0016-7037(96)00091-9.

Blowes, D. W., & Ptacek, C. J. (1994). Acid-neutralization mechanisms. In J. L. Jambor, & D. W. Blowes (Eds.), *Short course handbook on environmental geochemistry of sulphide mine-wastes* (pp. 271–292). Ontario: Mineralogical Association of Canada.

Borrego, J., Morales, J. A., De la Torre, M. L., & Grande, J. A. (2002). Geochemical characteristics of heavy metal pollution in surface sediments of the Tinto and Odiel river estuary (southwestern Spain). *Environmental Geology*, *41* (7), 785–796. doi:10.1007/s00254-001-0445-3.

Boski, T., Moura, D., Veiga-Pires, C., Camacho, S., Duarte, D., Scott, D. B., & Fernandes, S. G. (2002). Postglacial sea-level rise and sedimentary response in the Guadiana Estuary, Portugal/Spain border. *Sedimentary Geology*, *150*, 103–122. doi:10.1016/S0037-0738(01)00270-6.

Bryan, C. G., Hallberg, K. B., & Johnson, D. B. (2006). Mobilisation of metals in mineral tailings at the abandoned Sao Domingos copper mine (Portugal) by indigenous acidophilic bacteria. *Hydrometallurgy*, *83*, 184–194. doi:10.1016/j.hydromet.2006.03.023.

Cánovas, C. R., Olías, M., Nieto, J. M., Sarmiento, A. M., & Cerón, J. C. (2007). Hydrogeochemical characteristics of the Tinto and Odiel Rivers (SW Spain). Factors controlling metal contents. *The Science of the Total Environment*, *373*, 363–382. doi:10.1016/j.scitotenv.2006.11.022.

Capelo, J. H. (1996). Esboço da paisagem vegetal da bacia Portuguesa do Rio Guadiana. *Silva Lusitana*, IV(número especial), 13–64.

Carlson, L., & Schwertmann, U. (1981). Natural ferrihydrites in surface deposits from Finland and their association with silica. *Geochimica et Cosmochimica Acta*, *45*, 421–429. doi:10.1016/0016-7037(81)90250-7.

Davis, J. (1986). *Statistical and data analysis in geology* p. 646. Singapore: Wiley.

Delgado, J., Condesso de Melo, M. T., & Barrosinho, J. (2007). Physical–chemical characteristics of the superficial waters affected by acid mine drainage in the southern sector of the Guadiana basin (South-western of the Iberian Peninsula). *Geogaceta*, *42*, 55–58.

Delgado, J., Melo, M. T. C. d., Sarmiento, A. M., Nieto, J. M., & Barrosinho, J. (2006). Characterization of the pollution sources in surface and estuarine waters from the lower section of the Guadiana river basin (SW Iberian Peninsula). *34 Congress of International Association of Hydrogeologists*, 437–438, Beijing, China.

Dold, B. (2003). Dissolution kinetics of schwertmannite and ferrihydrite in oxidized mine samples and their detection by differential X-ray diffraction (DXRD). *Applied Geochemistry*, *18*, 1531–1540. doi:10.1016/S0883-2927(03)00015-5.

Elbaz-Poulichet, F., Braungardt, C., Achterberg, E., Morley, N., Cossa, D., Beckers, J. M., Nomerange, P., Cruzado, A., & Leblanc, M. (2001). Metal biogeochemistry in the Tinto–Odiel rivers (Southern Spain) and in the Gulf of Cadiz: a synthesis of the results of TOROS project. *Continental Shelf Research*, *21*(18–19), 1961–1973. doi:10.1016/S0278-4343(01)00037-1.

Freitas, H., Prasad, M. N. V., & Pratas, J. (2004). Plant community tolerant to trace elements growing on the degraded soils of Sao Domingos mine in the south east of Portugal: environmental implications. *Environment*

International, *30*, 65–72. doi:10.1016/S0160-4120(03)00149-1.

Gerhardta, A., Janssens de Bisthovena, L., & Soares, A. M. V. M. (2004). Macroinvertebrate response to acid mine drainage: community metrics and on-line behavioural toxicity bioassay. *Environmental Pollution*, *130*, 263–274. doi:10.1016/j.envpol.2003.11.016.

Grande, J. A., Beltrán, R., Sáinz, A., Santos, J. C., de la Torre, M. L., & Borrego, J. (2005). Acid mine drainage and acid rock drainage processes in the environment of Herrerías Mine (Iberian Pyrite Belt, Huelva-Spain) and impact on the Andévalo Dam. *Environmental Geology*, *47*, 185–196. doi:10.1007/s00254-004-1142-9.

Hudson-Edwards, K. A., Schell, C., & Macklin, M. G. (1999). Mineralogy and geochemistry of alluvium contaminated by metal mining in the Rio Tinto area, southwest Spain. *Applied Geochemistry*, *14*, 1015–1030. doi:10.1016/S0883-2927(99)00008-6.

Jerz, J. K., & Rimstidt, J. D. (2003). Efflorescent iron sulfates minerals: Paragenesis, relative stability, and environmental impact. *The American Mineralogist*, *18*, 1919–1932.

Kawano, M., & Tomita, K. (2001). Geochemical modelling of bacterially induced mineralization of schwertmannite and jarosite in sulfuric acid spring water. *The American Mineralogist*, *86*, 1156–1165.

Loureiro, J. M. (1983). Monografia Hidrológica do Algarve. Universidad del Algarbe, Dirección general de Recursos y Aprovechamientos Hidráulicos (pp. 17).

Morales, J. A. Sedimentología del Estuario del Río Guadiana (SO España-Portugal). (1993). Ph.D. thesis, University of Sevilla (pp. 300).

Murad, E., & Rojik, P. (2003). Iron-rich precipitates in a mine drainage environment: influence of pH on mineralogy. *The American Mineralogist*, *88*, 1915–1918.

Nocete, F., Álex, E., Nieto, J. M., Sáez, R., & Bayona, M. R. (2005). An archaeological approach to regional environmental pollution in the south-western Iberian Peninsula related to third millennium BC mining and metallurgy. *Journal of Archaeological Science*, *32*, 1566–1576. doi:10.1016/j.jas.2005.04.012.

Nordstrom, D. K. (1982). The effect of sulfate on aluminum concentrations in natural waters: some stability relation in the system Al2O3-SO3-H2O at 298 K. *Geochimica et Cosmochimica Acta*, *46*, 681–692. doi:10.1016/0016-7037(82)90168-5.

Nordstrom, D. K., & Alpers, C. N. (1999). Geochemistry of acid mine waters. In G. S. Plumlee, M. J. Logson (Eds), *The environmental geochemistry of mine waters 6A. Rev. Econ. Geol.* (pp. 133–160). Littleton, CO: Society of Economic Geology.

Nordstrom, D. K., & Wilde, F. D. (1998). Reduction–oxidation potential (electrode method). U.S. Geological Survey Techniques of Water-Resources Investigations, book 9, chap. A6., section 6.5, pp. 20.

Olías, M., Cánovas, C. R., Nieto, J. M., & Sarmiento, A. M. (2006). Evaluation of the dissolved contaminant load transported by the Tinto and Odiel rivers (South West Spain). *Applied Geochemistry*, *21*, 1733–1749. doi:10.1016/j.apgeochem.2006.05.009.

Olías, M., Nieto, J. M., Sarmiento, A. M., Cerón, J. C., & Cánovas, C. R. (2004). Seasonal water quality variations in a river affected by acid mine drainage: the Odiel River (South West Spain). *The Science of the Total Environment*, *333*, 267–281. doi:10.1016/j.scitotenv.2004.05.012.

Parkhurst, D. L., & Appelo, C. A. J. (1999). User's guide to PHREEQC (Version 2)—A computer program for speciation, batch reaction, one-dimensional transport, and inverse geochemical calculations. *USGS water-resources investigations report 99–4259* (pp. 312). Denver: U.S. Geological Survey.

Perona, E., Bonilla, I., & Mateo, P. (1999). Spatial and temporal changes in water quality in a Spanish river. *The Science of the Total Environment*, *241*, 75–90. doi:10.1016/S0048-9697(99)00334-4.

Plumlee, G. S., Smith, K. S., Ficklin, W. H., & Briggs, P. H. (1992). Geological and geochemical controls on the composition of mine drainages and natural drainages in mineralized areas. *Proceeding presented at the 7th International Water-Rock Interaction Conference, Park City, Utah*.

Regenspurg, S., Brand, A., & Peiffer, S. (2004). Formation and stability of schwertmannite in acidic mining lakes. *Geochimica et Cosmochimica Acta*, *68*, 1185–1197. doi:10.1016/j.gca.2003.07.015.

Rivas-Martínez, S., Lousa, M., Díaz, T. E., Fernández-González, F., & Costa, J. C. (1990). La vegetación del sur de Portugal (Sado, Alentejo y Algarve). *Itinera Geobotanica*, *3*, 5–126.

Sáez, R., Pascual, E., Toscano, M., & Almodóva, G. R. (1999). The Iberian type of volcano-sedimentary massive sulphide deposits. *Mineralium Deposita*, *34*, 549–570. doi:10.1007/s001260050220.

Sainz, A., Grande, J. A., De La Torre, M. L., & Sánchez-Rodas, D. (2002). Characterisation of sequential leachate discharges of mining waste rock dumps in the Tinto and Odiel rivers. *Journal of Environmental Management*, *64* (4), 345–353. doi:10.1006/jema.2001.0497.

Sánchez-España, J., Lopez-Pamo, E., Santofimia, E., Aduvire, O., Reyes, J., & Barettino, D. (2005a). Acid mine drainage in the Iberian Pyrite Belt (Odiel river watershed, Huelva, SW Spain): Geochemistry, mineralogy and environmental implications. *Applied Geochemistry*, *20*, 1320–1356. doi:10.1016/j.apgeochem.2005.01.011.

Sánchez-España, J., Lopez-Pamo, E., Santofimia, E., Reyes, J., & Martín, J. A. (2005b). The natural attenuation of two acidic effluents in Tharsis and La Zarza-Perrunal mines (Iberian Pyrite Belt, Huelva, Spain). *Environmental Geology*, *49*, 253–266. doi:10.1007/s00254-005-0083-2.

Sánchez-España, J., Lopez-Pamo, E., Santofimia, E., Reyes, J., & Martín, J. A. (2006a). The impact of acid mine drainage on the water quality of the Odiel River (Huelva, Spain): evolución of precipitate mineralogy and aqueous geochemistry along the Concepción-Tintillo segment. *Water, Air, and Soil Pollution*, *173*, 121–149. doi:10.1007/s11270-005-9033-6.

Sánchez-España, J., Lopez-Pamo, E., Santofimia, E., Reyes, J., & Martín, J. A. (2006b). The removal of dissolved metals by hydroxysulphates precipitates during oxidation and neutralization of acid mine waters, Iberian Pyrite Belt. *Aquatic*

Geochemistry, *12*, 268–298. doi:10.1007/s10498-005-6246-7.

Sarmiento, A. M. (2008). Study of the pollution by acid mine drainage of the surface waters in the Odiel basin (SW Spain). Ph.D. thesis, Univ. Huelva. ProQuest LLC (pp. 352).

Sarmiento, A. M., Nieto, J. M., & Olías, M. (2004). The contaminant load transported by the river Odiel to the Gulf of Cádiz (SW Spain). *Transactions of the Institution of Mining and Metallurgy Section B. Applied Earth Science*, *113*, 117–122. doi:10.1179/037174504225005690.

Sarmiento, A. M., Nieto, J., Olías, M., & Cánovas, C. R. (2006). Pollution of a river basin impacted by acid mine drainage in the Iberian Pyrite Belt (SW Spain). *7th International Conference on Acid Rock Drainage*, Abstract vol.1, 1850–1862).

Tyler, G., Carrasco, R., Nieto, J. M., Pérez, R., Ruiz, M. J., & Sarmiento, A. M. (2004) Optimization of major and trace element determination in acid mine drainage samples by ultrasonic nebulizer-ICP-OES (USNICP-OES). Pittcon 2004 conference, Chicago, CD-ROM, Abst. # 9000-1000.

Williams, D. J., Bigham, J. M., Cravotta, C. A., Traina, S. J., Anderson, J. E., & Lyon, J. G. (2002). Assessing mine drainage pH from the color and spectral reflectance of chemical precipitates. *Applied Geochemistry*, *17*, 1273–1286. doi:10.1016/S0883-2927(02)00019-7.

Yu, J. Y., Heo, B., Choi, I. K., Cho, J. P., & Chang, H. W. (1999). Apparent solubilities of schwertmannite and ferrihydrite in natural stream waters polluted by mine drainage. *Geochimica et Cosmochimica Acta*, *63*, 3407–3416. doi:10.1016/S0016-7037(99)00261-6.